JCTC Journal of Chemical Theory and Computation

Article

pubs.acs.org/JCTC

Long-Time-Step Molecular Dynamics through Hydrogen Mass Repartitioning

Chad W. Hopkins,[†] Scott Le Grand,[‡] Ross C. Walker,[§] and Adrian E. Roitberg*[,∇]

[†]Department of Physics, Quantum Theory Project, University of Florida, Gainesville, Florida 32611, United States

[‡]Amazon Web Services, 2201 Westlake Ave., Suite 500, Seattle, Washington 98121, United States

[§]San Diego Supercomputer Center & Department of Chemistry and Biochemistry, University of California San Diego, 9500 Gilman Drive, MC0505, La Jolla, California 92093-0505, United States

[∇]Department of Chemistry, Quantum Theory Project, University of Florida, Gainesville, Florida 32611, United States

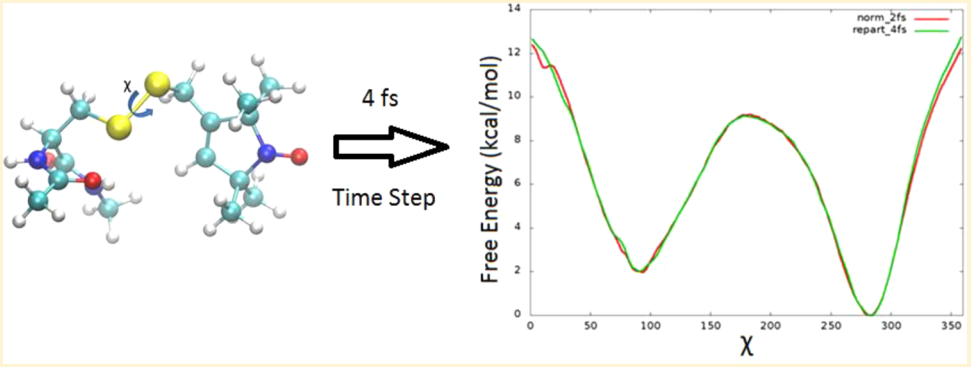

ABSTRACT: Previous studies have shown that the method of hydrogen mass repartitioning (HMR) is a potentially useful tool for accelerating molecular dynamics (MD) simulations. By repartitioning the mass of heavy atoms into the bonded hydrogen atoms, it is possible to slow the highest-frequency motions of the macromolecule under study, thus allowing the time step of the simulation to be increased by up to a factor of 2. In this communication, we investigate further how this mass repartitioning allows the simulation time step to be increased in a stable fashion without significantly increasing discretization error. To this end, we ran a set of simulations with different time steps and mass distributions on a three-residue peptide to get a comprehensive view of the effect of mass repartitioning and time step increase on a system whose accessible phase space is fully explored in a relatively short amount of time. We next studied a 129-residue protein, hen egg white lysozyme (HEWL), to verify that the observed behavior extends to a larger, more-realistic, system. Results for the protein include structural comparisons from MD trajectories, as well as comparisons of pK_a calculations via constant-pH MD. We also calculated a potential of mean force (PMF) of a dihedral rotation for the MTS [(1-oxyl-2,2,5,5-tetramethyl-pyrroline-3-methyl)methanethiosulfonate] spin label via umbrella sampling with a set of regular MD trajectories, as well as a set of mass-repartitioned trajectories with a time step of 4 fs. Since no significant difference in kinetics or thermodynamics is observed by the use of fast HMR trajectories, further evidence is provided that long-time-step HMR MD simulations are a viable tool for accelerating MD simulations for molecules of biochemical interest.

I. INTRODUCTION

For conventional MD simulations of large biomolecules in explicit solvent, the edge of the current simulation time scale available for routine access with modest computational resources lies roughly in the range of hundreds of nanoseconds, with the recent introduction of GPU accelerated code pushing this limit toward microseconds.[1−4] Running for this amount of simulation time still involves a substantial real-time investment. In addition, multiple long trajectories are often required for an appropriate statistical analysis for large systems, and many processes of biological importance take place on the time scale of at least hundreds of microseconds.[2,5] Thus, improving on this "sampling problem" of MD is an important challenge that has been faced with a variety of techniques (see, for example, a recent review by Christ et al.[6] and the recent work by Hansen and Hünenberger,[7] and references cited therein).

The length of a simulation is defined in units of the time step employed in the integration of the equations of motion. The size of the time step of an MD simulation is constrained by the time scale of the highest frequency motion in the system. This is typically bond vibrations involving hydrogen atoms; the often-quoted 1-fs limit is due to these fast vibrations. Increasing the time step beyond this number potentially makes the simulation unstable, with a higher probability of instabilities appearing the longer that the simulation is run. The 1-fs limit is

Received: November 21, 2014
Published: March 16, 2015

DOI: 10.1021/ct5010406
J. Chem. Theory Comput. 2015, 11, 1864−1874

commonly combated with the introduction of restraints on the high-frequency bonds. In Amber,[8] the most common simulation setup involves the application of the SHAKE[9] algorithm to nonwater bonds involving hydrogens, and the analytic SETTLE[10] algorithm to water bonds and angles, with a time step of 2 fs. This 2-fs limit is due to limitations in the SHAKE algorithm itself.

Apart from simulation stability issues, there are also formal issues with increasing the time step. The velocity Verlet/leapfrog family of integrators has an error, when taken over the entire trajectory, that is second order with regard to the time step.[11] Practically, what this means is that (i) different time steps lead to different trajectories, and (ii) the larger the time step, the further the computed trajectory deviates from the "correct" one prescribed by Newtonian mechanics. This is only a problem if the ensemble sampled from the frames of the trajectory is significantly altered from the original ensemble, thus changing any observables calculated over the entire trajectory. In fact, symplectic integrators, such as Velocity Verlet and Leapfrog, have been shown to give the exact solution to a so-called "shadow Hamiltonian", which can be expressed as a Taylor expansion in the time step.[12−14] This allows one to, in theory, analytically express the error introduced into the system energy by the size of the time step, and predict the effect on the sampled ensemble. In practice, this type of analysis has been used to predict the energy drift seen in NVE simulations.[12] However, employing a thermostat in an NVT or NPT simulation, as is more widely used, tends to obfuscate the problem. For instance, NVT simulations do not usually suffer from the same type of energy drift seen in NVE simulations.[15] This is dependent on the type of thermostat algorithm employed; in some sense, with some thermostats, accumulating discretization errors in the total system energy is "fixed" by siphoning out excess energy introduced by the integrator into the heat bath. For some thermostats, conserved energies can be defined that allow the same type of time step error analysis as with microcanonical simulations. Still, the formal description of the discretization error becomes more difficult with a thermostat. There has been some work to this end, particularly with the use of Langevin dynamics as a thermostat.[16,17] In this manuscript, we take a more empirical approach in showing that the longer-time-step MD trajectories that we employ do not introduce significant discretization errors, and do not attempt to provide a formal theoretical framework for the method.

With these two limitations (simulation stability and formal discretization error) in mind, we turn to hydrogen mass repartitioning (HMR) as a method to increase the time step of the MD simulation by a factor of 2, while keeping within the bounds set by both limitations. The idea of changing atomic masses in order to speed up MD simulations has been around since at least the 1970s.[18] The main idea behind the method is that equilibrium thermodynamic averages of observables are not dependent on the exact mass distribution of the system. For the canonical ensemble, these averages take the form

$$\langle A \rangle = \frac{\int A e^{-\beta \mathcal{H}} \, dp \, dx}{\int e^{-\beta \mathcal{H}} \, dp \, dx}$$

If $A = A(x)$ and the Hamiltonian is separable in position and momentum, as is the case with MD with classical force fields without magnetic terms, then the momentum-dependent parts of the integrals on the top and bottom can be separated out and thus cancel. Assuming that the force field does not contain any mass-dependent terms, the remaining expression is independent of the mass distribution of the system.

Some early work actually focused on employing a general mass tensor to the kinetic energy part of the Hamiltonian, with entries calculated from a normal modes analysis of the system,[19] which has branched into a separate line of inquiry that we will not focus further on here. Over the next decades, a few studies[20−24] were conducted that involved simply increasing the masses of the hydrogen atoms (or, in some cases, every atom) in the system in order to slow down their motion. The results from these studies were promising, displaying the ability to speed up MD simulations by a factor of ∼10, seemingly. However, Feenstra et al.[25] pointed out that increasing the total system mass by selectively changing atomic masses in this way actually scales the time of the simulation, so that reported simulation lengths are offset by a factor that is related to the ratio of system masses between the original and changed systems. In this seminal study, Feenstra et al. prescribed the repartitioning of mass among the atoms in the system, so that the total system mass is kept constant. In other words, the mass of the light hydrogen atoms is increased while the masses of the heavy atoms are decreased by the same amount. This study became the basis for several implementations of the HMR technique, particularly in the GROMACS[26] and ACEMD[27] programs. In the years since ref 25, there have been few works that builded on this initial survey; in fact, one of the more recent studies, by Rao and Spichty, did not use HMR, but rather applied the older method of increasing the mass of only the solute hydrogens.[28] The longest simulation that was run in ref 25 was 1 ns. With modern hardware, it is possible to study the effects of long-time-step HMR MD on trajectories of hundreds of nanoseconds, which is our focus here. It is important to show that a lengthened time step using HMR does not introduce significant errors in long simulations, and can indeed keep the simulation stable over long time scales.

The rest of this manuscript will be organized as follows. In Section II, the details of the MD simulations analyzed with HMR will be described. Section III gives the results of our tests and provides discussion on the results. Section IV provides further discussion on HMR. We conclude in section V.

II. METHODS

Mass Repartitioning. A slightly different mass repartitioning scheme than that used in previous studies was employed in our investigation. The scheme of ref 25 scales all hydrogen masses by a factor of 4, while decreasing the masses of the bonded heavy atoms by enough to keep the total system mass constant. Because of technical reasons with the GPU code in Amber, we use a scaling factor of 3. This factor is also more satisfactory when applied to methyl groups, because a scaling factor of 4 leads to the methyl carbon having a lower mass (3 amu) than the methyl hydrogens (4 amu). Figure 1 shows how this scheme is applied to alanine dipeptide. Three different mass topology schemes were studied: normal masses ("norm"), HMR applied to only the solute atoms ("repart"), and HMR applied to the solute and solvent atoms ("repart_water"). The application of the analytic SETTLE algorithm, and the total absence of high-frequency intramolecular movement in the TIP3P model means that the water molecules can already be simulated at a higher time step than 2 fs without affecting simulation stability; how this affects discretization error does not have a clear *a priori* answer.

DOI: 10.1021/ct5010406
J. Chem. Theory Comput. 2015, 11, 1864−1874

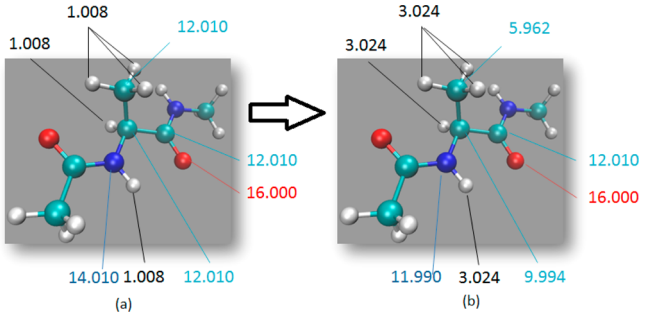

Figure 1. Example of the HMR scheme used in this study applied to alanine dipeptide; masses (in amu) shown for the original system (a) before mass repartitioning and (b) after applying HMR. Note that the total system mass is not changed by applying HMR.

All MD simulations were performed with the CUDA accelerated Amber 14 program.[4,8,29,30] Peptide and protein force field parameters were obtained from the ff12SB force field (a newer revised version of the ff99SB[31,32] force field), and the original MTS spin label parameters came from GAFF,[33] with charges derived from a RESP[34] fit using an HF/6-31G* electrostatic potential calculated using the Gaussian 09 program.[35] The five linking dihedrals in the spin label model, including χ, were reparameterized via a simultaneous five-dimensional fit with MP2/6-31G*//HF/6-31G* data, using our previously reported dihedral parametrization method.[36] All trajectories were analyzed with the cpptraj[37] program in Amber.

Peptide. The first system that will be presented is a small capped peptide, $(Ala)_3$ (see Figure 2a). The structure was built

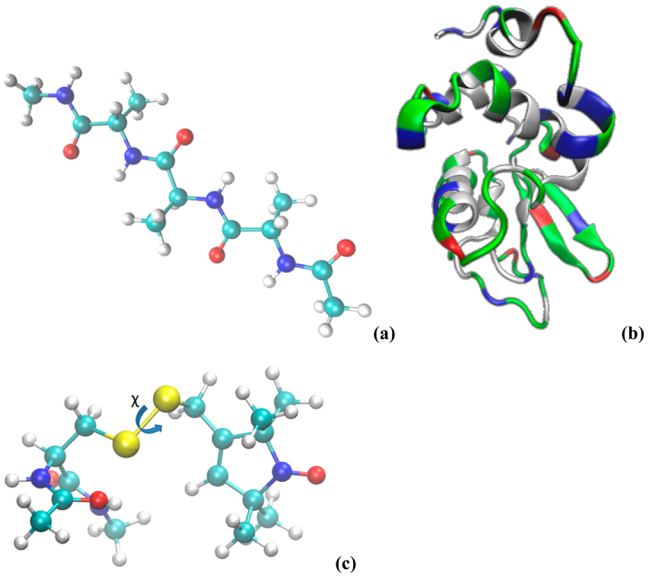

Figure 2. Structures of systems studied: (a) capped $(Ala)_3$, (b) HEWL protein, and (c) MTS spin label model.

and solvated with the LEaP Amber program with an octahedral box, leading to the addition of 1106 TIP3P[38] water residues, for a total of 3360 total atoms. Because of the small size of the solute, stable MD trajectories can be run for this system with time steps of up to 4 fs with normal masses and 5 fs with HMR applied. We will further explore what happens beyond these time steps in Section IV. Ten trajectories were run for each time step of 1, 2, 3, and 4 fs for the "norm" mass topology, and for time steps of 1, 2, 3, 4, and 5 fs for the "repart" and "repart_water" topology types, giving 140 total trajectories. Each trajectory was independently equilibrated, consisting of minimization, 200 ps of heating to 300 K, and 100 ps of density equilibration with a constant pressure simulation. From the equilibrated structure, each trajectory was run for 450 ns of NVT production time, with energies and structures saved every 0.48 ps. In all production runs in this study, all covalent hydrogen bonds were restrained with SHAKE/SETTLE, and Langevin dynamics with a weak coupling (collision frequency of 1 ps^{-1}) was used as a thermostat.

Protein Structure. The initial HEWL structure (Figure 2b) was obtained from a crystal structure (Protein Data Bank (PDB) ID: 4LYT).[39] With LEaP, eight Cl^- counterions were added to neutralize the protein's total charge; the resulting structure was solvated with an octahedral box, with 5736 TIP3P water residues added for a total of 19 152 atoms. With the protein, only trajectories with time steps up to 3 fs for normal masses and 4 fs with HMR were stable. Fifteen trajectories were run for time steps of 1, 2, and 3 fs for the norm topology and for time steps of 1, 2, 3, and 4 fs for the repart and repart_water topologies, giving 165 total trajectories. For the protein, a common equilibrated structure was used as a starting point for all trajectories, equilibrated through a similar process to the peptide, with 2 ns of additional NVT equilibration time. Each trajectory was then run for 160 ns of production time in the NVT ensemble, with energies and structures saved every 12 ps.

Protein−pK_a. The option to run constant pH MD simulations[40] was recently added to the GPU accelerated Amber code. We also investigated the effect of long-time-step HMR trajectories on the calculation of pK_a values for titratable residues in HEWL using this feature. To this end, we ran two sets of trajectories (2-fs time step with norm mass topology and 4-fs time step with the repart topology) with ten residues specified as targets for attempted protonation state changes in the Generalized Born implicit solvent model. These were run for pH values from 0 to 7 in pH increments of 0.5, with 20 independent trajectories run for each pH value, starting from a common equilibrated structure. Each trajectory was run for 50 ns, with protonation state changes attempted every three MD steps. Titration curves for each trajectory set were derived through the calcpka program in Amber. pK_a values were then calculated by fitting the modified Hill equation to the titration curve:

$$f_d = \frac{1}{1 + 10^{n(\mathrm{p}K_a - \mathrm{pH})}}$$

This fit was performed by algebraically minimizing the least-squares term of f_d to the data.

Spin Label. The MTS spin label has been used to study protein dynamics (e.g., flap movement in the HIV-1 protease[41]) in EPR experiments and has previously been the target for force field parametrization efforts,[42] as accurately characterizing the dynamics of the label, particularly movement in the flexible chain linking the spin label to the protein, is important for interpreting EPR measurements. The model that we use for the spin label is a single-capped cysteine residue attached to the spin label via a disulfide bond (Figure 2c). The model's initial structure was built with the Vega ZZ[43] modeling software, and solvated in LEaP with 848 TIP3P water residues, for a total atom count of 2593. The resulting system was equilibrated using the same process as for the peptide. The barrier to rotation about the linking dihedral centered on the disulfide bond (labeled χ in the figure) was then analyzed via umbrella

DOI: 10.1021/ct5010406
J. Chem. Theory Comput. 2015, 11, 1864−1874

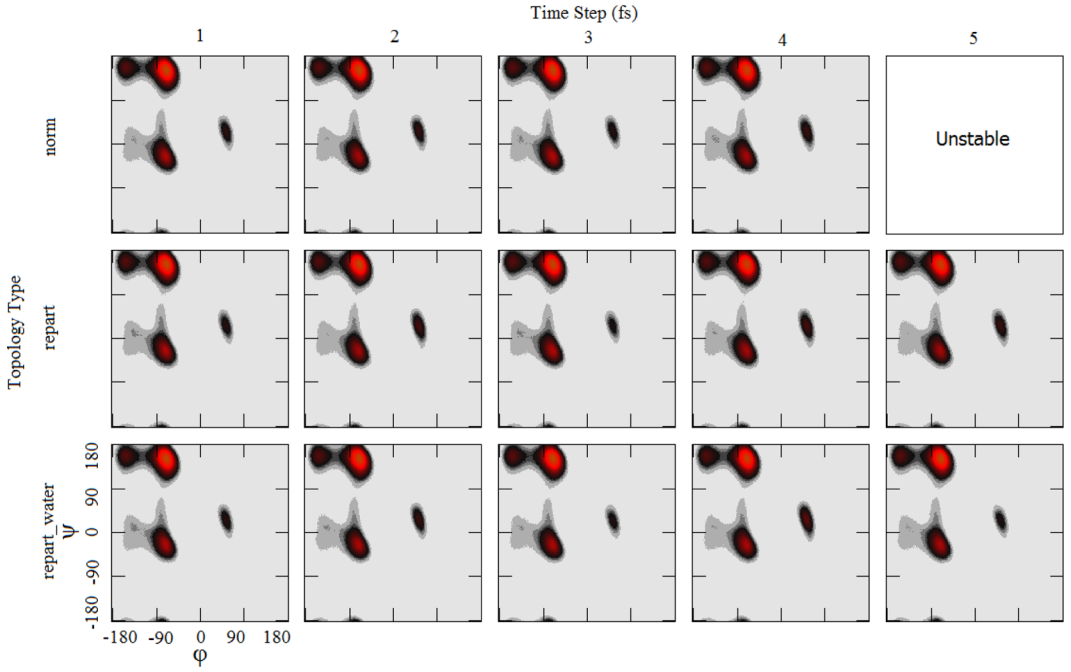

Figure 3. Population statistics of central φ/ψ angles in the $(Ala)_3$ peptide for different time step and mass topology combinations. Axis scale shown in lower left plot. Note that configurations which accounted for $<10^{-3}$ % of the total time were culled from the plot, and that all plots are shown on the same color scale.

sampling. We used 120 windows of 7.5×10^4 biased MD steps, with the centers of bias for the windows equally spaced over the full 360° range of rotation. Two trajectory types were run for this test: 2 fs time step (150 ps per window) with the norm topology and 4 fs time step (300 ps per window) with the repart topology. The weighted histogram analysis method (WHAM)[44] was then used to remove the effect of the bias in the individual windows and produce a single PMF for the dihedral.

III. RESULTS

Peptide. We studied the dynamics of the peptide, in terms of the three sets of φ/ψ angles along the length of the molecule. Figure 3 shows the accumulated population statistics for the middle (i.e., spanning the second alanine residue) φ/ψ angles of the peptide, integrated over all other degrees of freedom, taken over all 10 trajectories for each time step/topology combination.

As can be seen in the figure, the Ramachandran populations are remarkably similar. The root mean square (RMS) error between the norm/1 fs populations and the other topology/time step combinations are as follows (in units of $\times 10^{-4}$ %):

- for the norm topology, 2−4 fs: 1.46, 1.57, 1.82
- for the repart topology, 1−5 fs: 1.35, 1.93, 1.61, 2.21, 2.30
- for the repart_water topology, 1−5 fs: 1.36, 1.62, 1.44, 3.26, 1.59

It is somewhat surprising that the same level of agreement extends to the 4 fs (norm topology) and 5 fs (repart and repart_water topologies) trajectories, since these time steps are higher than usually prescribed by NVE energy drift studies. Here, we also note that the real wall times to run the longer-time-step simulations for the same amount of simulation time (450 ns) were shorter. The 5-fs trajectories ran in about one-fifth of the time as the 1-fs trajectories. The main comparison of interest, the norm/2 fs trajectories to the repart/4 fs (or repart_water/4 fs) trajectories, represents an approximate doubling of throughput.

For a more in-depth investigation of the sampling in each trajectory type, we defined three semistable conformations for each alanine residue: β-sheet (β) (combining the canonical β sheet and poly proline II conformations), right-handed α-helix (α_R), and left-handed α-helix (α_L). We investigated the relative sampling and kinetics among the 27 unique rotamers defined by the permutations of these three local conformations in each of the three alanine residues. A definition of "semi-stable" was derived based on free energies calculated over the 10 norm/1 fs trajectories, for the central φ/ψ coordinates. A cutoff of 2 kcal/mol was applied to this two-dimensional (2D) free-energy surface to define a φ/ψ "mask" (Figure 4); every configuration in φ/ψ space for that particular residue that had a free energy less than the cutoff was considered to be semistable. For each trajectory frame, the mask was applied to each alanine residue, and if the conformation of all three residues fell within the mask, that frame was marked as a semistable rotamer and categorized into one of the 27 rotamer states based on the conformation of the individual alanine residues. Figure 5 shows the fractional populations for the four most populated of the 27 rotamers, averaged over the 10 trajectories for each trajectory type. Figure 6 shows average transition rates between rotamers for the transitions with the highest frequency. A transition was counted as soon as the peptide moved from one rotamer conformation to another; i.e., the given rates include transitions between the two rotamers along any pathway that did not contain another rotamer conformation.

The plots clearly show that there are no significant differences between the various topology/time step trajectory types, in terms of relative sampling. The main systematic variation that is noticeable in the population numbers is a slight downward drift with increasing time step, which is most easily visible in the highly populated N-(β−β−β)-C rotamer. With

DOI: 10.1021/ct5010406
J. Chem. Theory Comput. 2015, 11, 1864−1874

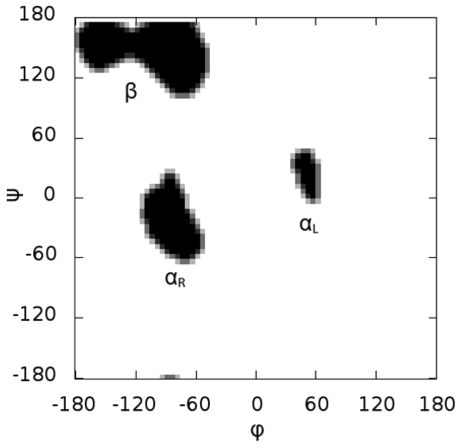

Figure 4. φ/ψ mask derived from norm/1 fs free energies. Regions of φ/ψ space colored black were considered semistable, and the mask was applied to each alanine residue in the peptide to define global rotamer conformations, based on the three local conformations shown (β, α_R, α_L).

increasing time step, the peptide spends slightly less time in the stable rotamer conformations. No systematic variation is observed from the application of HMR. Two trends are immediately apparent when comparing transition rates for all but the slowest transition shown. One shows a gradual increase in transition rate with time step. Also, the repart_water topology trajectories show a consistently lower rate for all transitions (~10% lower, on average). In other words, observed rates of interconversion among the rotamers were damped when applying HMR to the solvent. This agrees with observations from ref 25, which attribute a decrease in conformational space sampling efficiency when applying HMR to an increase in viscosity. In the repart trajectories, viscosity is not affected by HMR, and thus a similar sampling efficiency to the norm trajectories is observed. This conservation of sampling efficiency comes at the price of increased discretization error, at least in the solvent dynamics.

Typically, discretization error is more accurately monitored by calculating energy drift in an NVE simulation. As previously mentioned, constant temperature simulations do not express discretization error in the same way as NVE simulations; there is no energy drift during the course of the trajectory. In terms of energetics, the most noticeable difference between trajectories with different time steps is the average potential energy; there is a shift toward higher energy with an increase in time step. This phenomenon has been noted before.[28] We reiterate that this is solely due to discretization error from the time step, and repartitioning masses with HMR does not lead to further energy increases. Figure 7 shows the average potential energies for each trajectory type, taken over all 10 trajectories for that type.

The repart_water topology type shows the most stable behavior with increasing time step, with a consistently lower potential energy for all time steps, compared to the other two topology types. This trend seems to indicate that errors in the

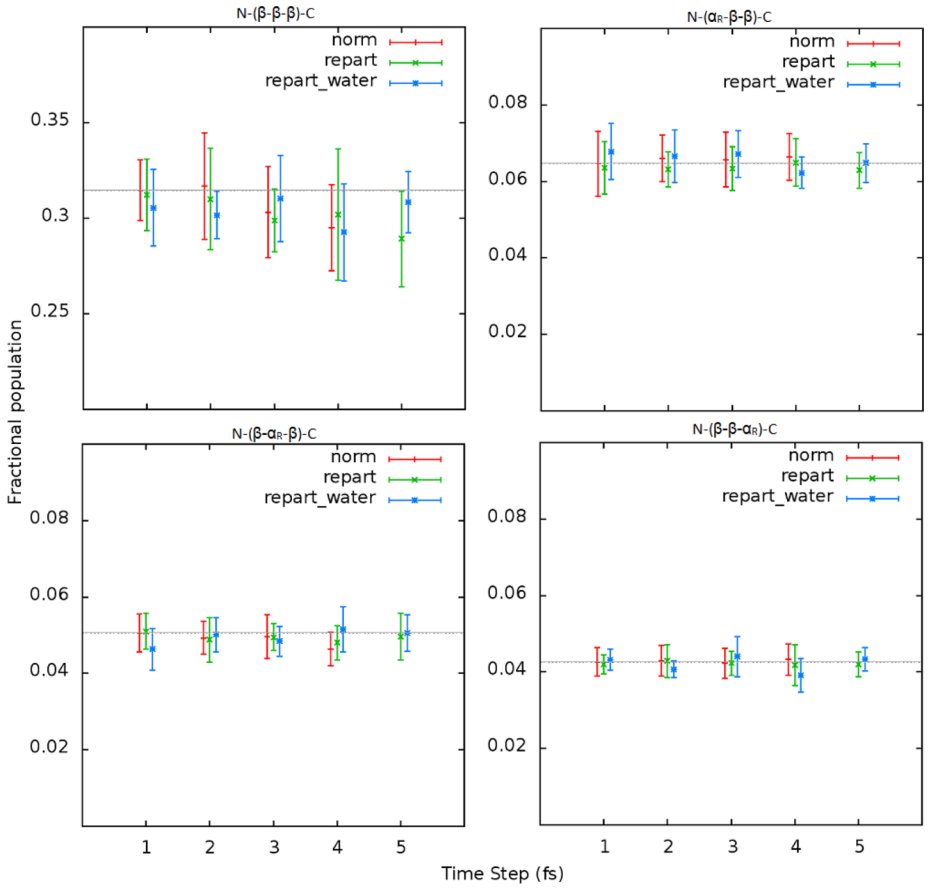

Figure 5. Fractional populations of the most populated rotamers in the $(Ala)_3$ peptide, averaged over 10 450-ns trajectories. Norm/1 fs average shown as a gray line for reference.

DOI: 10.1021/ct5010406
J. Chem. Theory Comput. 2015, 11, 1864−1874

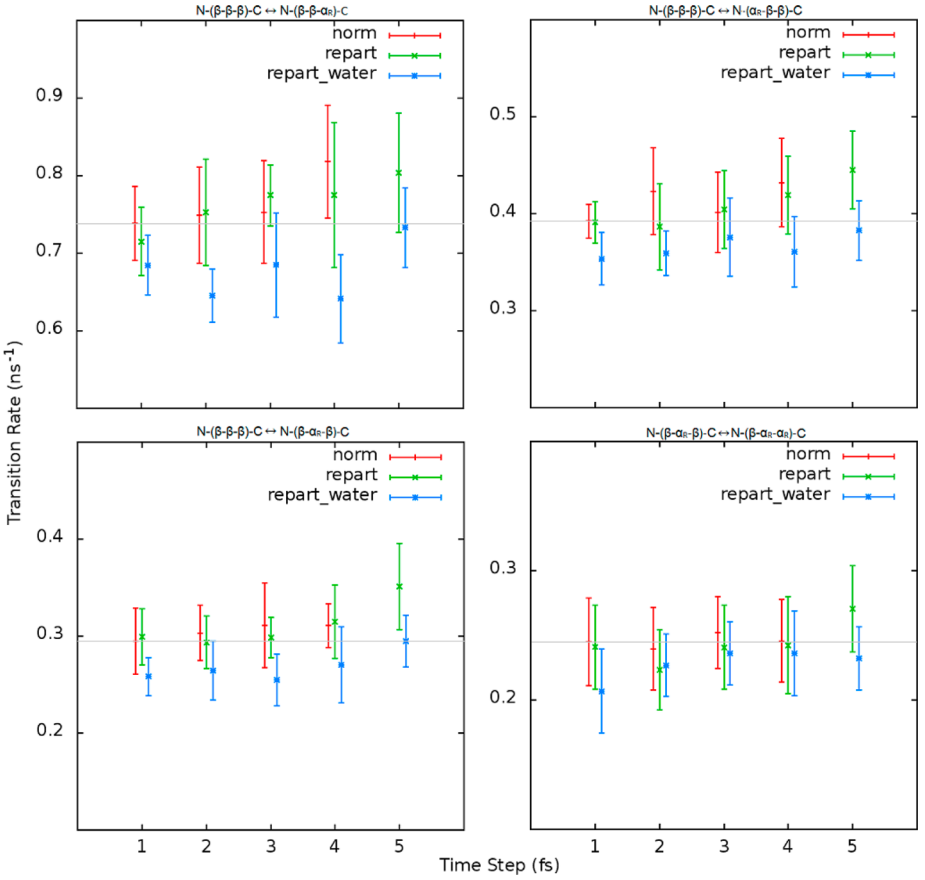

Figure 6. Average transition rates between rotamers with highest transition frequency in $(Ala)_3$ peptide. Norm/1 fs average shown as a gray line for reference.

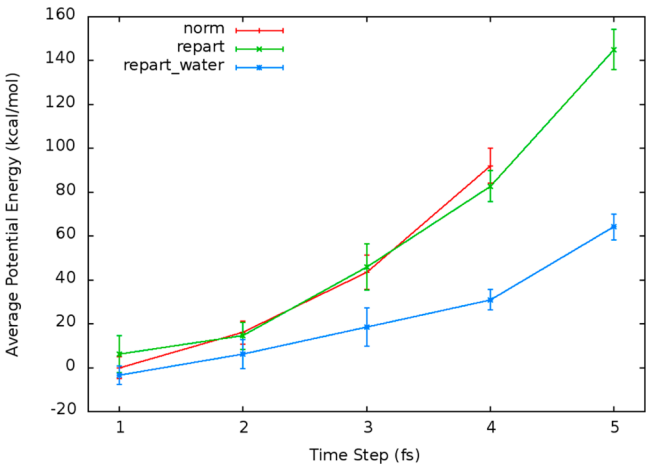

Figure 7. Average potential energies with different mass topology/time step combinations for the $(Ala)_3$ peptide, relative to the norm/1 fs average, averaged over 10 trajectories of each trajectory type. The error bars show the standard deviation in the mean over the 10 trajectories.

water librational motion are the main contributor to the shift in energy surface being explored. The repart_water topology damps the water librational motion with HMR, while the norm and repart topologies do not, which would explain the consistently lower potential energy that is observed for this topology.

Protein−Structure. Figure 8 shows a histogram of the total backbone root-mean-square deviation (RMSD) to the 4LYT

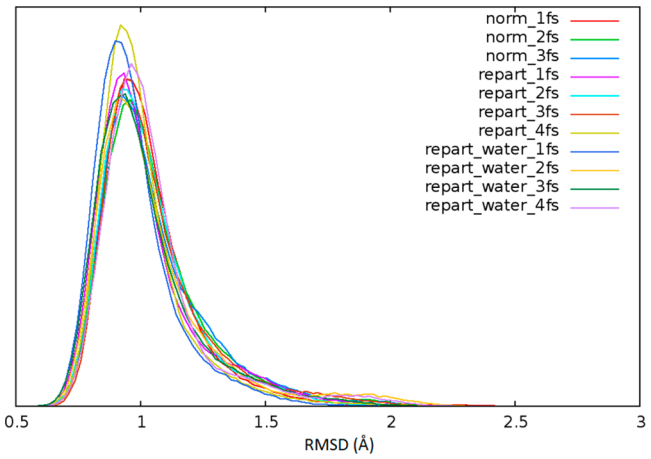

Figure 8. Backbone root-mean-square deviation (RMSD) to a crystal structure in HEWL for each trajectory type.

crystal structure for each of the trajectory types, taken over all 15 trajectories of each type. Figure 9a shows the per-residue RMSD to the same common structure, while Figure 9b shows the RMS fluctuations of the α-carbon in each residue, relative to its average position, over all trajectories of that type.

As with the peptide, there are no significant deviations in structure or flexibility observed by the application of HMR or

DOI: 10.1021/ct5010406
J. Chem. Theory Comput. 2015, 11, 1864−1874

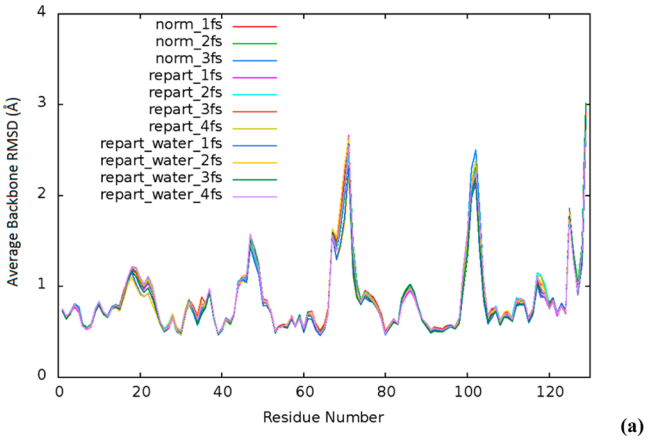

Figure 9. (a) Per-residue backbone RMSD to a crystal structure in HEWL. (b) Per-residue C_α RMS fluctuations against the average structure of each trajectory type.

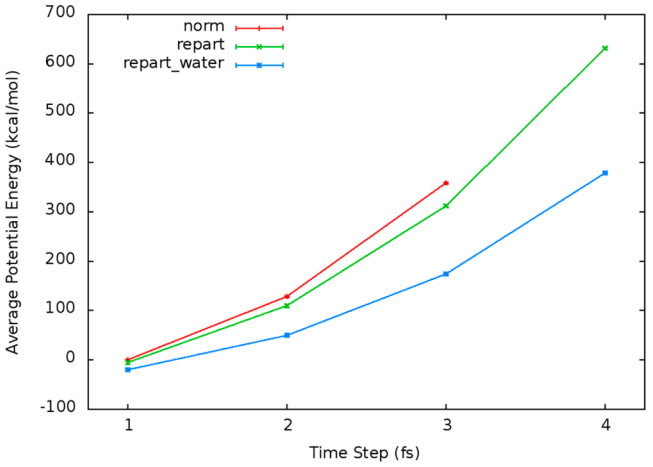

Figure 10. Average potential energies with different mass topology/time step combinations for HEWL, relative to the norm/1 fs average, averaged over 15 trajectories of each type.

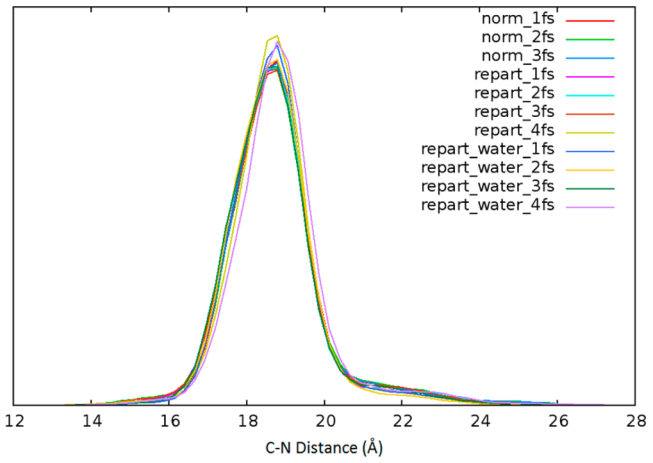

Figure 11. Terminal−terminal distance for HEWL averaged over each type of trajectory.

with the different time steps employed. The per-residue RMSD is particularly similar, while the RMS fluctuations show slightly more variation around the flexible random loops about residues 70 and 100; this can be attributed to a combination of lack of sampling and of biases in the different average structures being used for comparison. Figure 10 shows the average potential energy for each trajectory type taken over all 15 trajectories.

The relative shifts here are ∼6 times higher than those observed in the peptide, which corresponds roughly to the ratio of the system sizes. The relative behavior of the different topologies, with respect to increases in time step, is similar to the behavior observed with the peptide; in particular, once again, the repart_water topology shows the least increase in system energy with increasing time step.

To get a more specific view of the conformations being sampled in the protein system, Figure 11 shows the profile of the distance between the termini of the protein for each trajectory type. Again, no significant difference between the various trajectory types is observed. Another useful tool for exploring collective motions in proteins is the application of principal component analysis (PCA) to the backbone motion; this type of analysis has been previously employed to compare trajectories with different advanced sampling techniques (e.g., accelerated molecular dynamics[1]). The PCA functionality in cpptraj was used for the following analysis. PCA provides collective modes of the protein, ordered by their contribution to the variance of the motion over the entire trajectory. For each trajectory, PCA gives a set of eigenvectors corresponding to each mode obtained by diagonalizing the covariance matrix over the trajectory. It is expected that the eigenvectors between the different trajectory types, even from one trajectory to the next within the same type, will not be identical, as they are very sensitive to relatively small differences in the fluctuations from one trajectory to the next. However, these principal components (PCs) provide a worthwhile comparison by projecting the protein's motion over a trajectory onto a particular mode. We selected a single set of eigenvectors obtained from PCA on a single norm/1 fs trajectory, and used those as a basis set for comparing between trajectories. Figure 12 shows the projections onto the first four eigenvectors from this set for each trajectory type. We again note that the observed structure of the protein is independent of both the mass distributions and of the time steps employed in our tests.

Although eigenvectors obtained from PCA on one trajectory differ from those obtained from a different trajectory (even between trajectories of the same type), it is worthwhile to compare how well eigenvectors from one trajectory cover the space of a PC from a different trajectory. To this end, we investigated the behavior of eigenvector coverage versus number of eigenvectors in order to compare the various trajectory types, where we define eigenvector coverage, c, as

DOI: 10.1021/ct5010406
J. Chem. Theory Comput. 2015, 11, 1864−1874

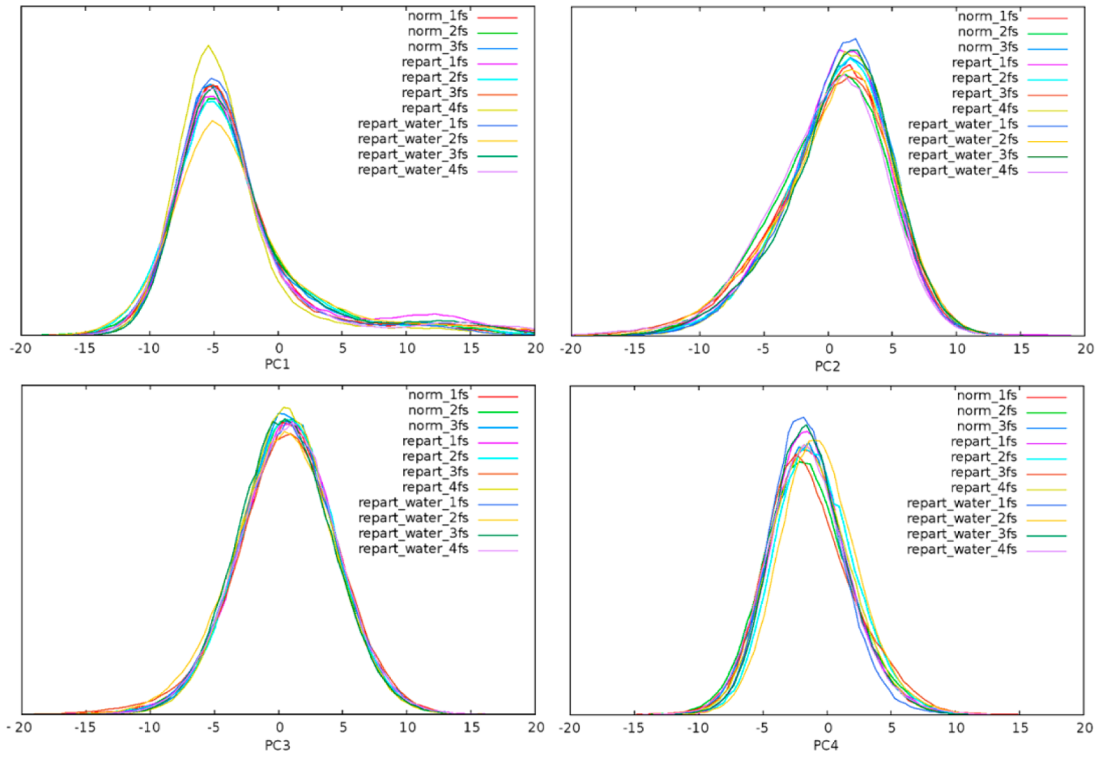

Figure 12. Projections of HEWL trajectories onto the top four eigenvectors from PCA on the protein backbone of a common norm/1 fs trajectory.

$$c = \sum_{i}^{N} (\vec{v}_o \cdot \vec{e}_i)^2$$

Here, $\vec{v}_o$ is the first eigenvector from the trajectory being used as a basis for comparison and the set $\vec{e}_i$ are the first N eigenvectors of the trajectory being compared. Figure 13 shows

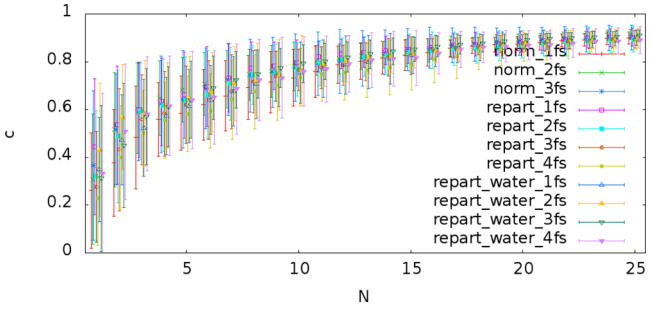

Figure 13. Plot of c vs N (see text) averaged over each type of trajectory. Note that error bars are shown for averaging over 15 trajectories for each trajectory type, except for norm/1 fs, for which 14 trajectories are used (one normal trajectory is used as the reference).

a plot of c vs N, averaged for each type of trajectory, using the first eigenvector from the previous reference set as $\vec{v}_o$. Again, the results show that using HMR and an increased time step does not affect the conformational ensemble, while increasing throughput (by a factor of 2, when comparing the norm/2 fs to the repart/4 fs and repart_water/4 fs trajectories).

Protein−pK_a. Figure 14 shows the evolution of the calculated pK_a values for 3 of the 10 targeted HEWL residues over the run time of the trajectories, in terms of invested processor time. Note that the actual wall time for these calculations was less, by a factor of 15, as the different pH values were run in parallel.

The two most interesting aspects to these plots are that (i) the norm/2 fs and repart/4 fs trajectories converge to the same pK_a within error, and (ii) the repart/4 fs trajectories converge approximately twice as fast as the norm/2 fs trajectories, which indicates that about half of the real calculation time is required to arrive at the same result. We note that, in the case of constant pH MD, one important degree of freedom—namely, the protonation state—is not being accelerated with the application of HMR with long time steps. This means that there are some cases where pK_a calculations, as shown here, will not necessarily converge more quickly from applying longer time steps to the configuration space sampling portion of the constant pH MD. However, this is a separate issue from the utility of long-time-step HMR MD.

Spin Label. Figure 15 shows the PMF calculated via WHAM for the linker dihedral, for the norm/2 fs and repart/4 fs trajectory types. The profiles are practically identical, in particular, the relative energies of the ±90° conformations and the barrier between them. The results here and with the pK_a calculations indicate that the increase in time step with HMR applied conserves relative conformational energies. Although the average sampled energy surface lies slightly above the original one, the relative global energetics of the studied systems appear to be unaffected.

IV. DISCUSSION

Using several examples, we have shown that HMR allows us to increase the MD time step without changing relative conformational sampling or kinetics of the trajectory. One further detail that is worth some comment is in the mixing of HMR with constraint algorithms, particularly SHAKE. In our tests on our largest system (HEWL), using the default Amber SHAKE

DOI: 10.1021/ct5010406
J. Chem. Theory Comput. 2015, 11, 1864−1874

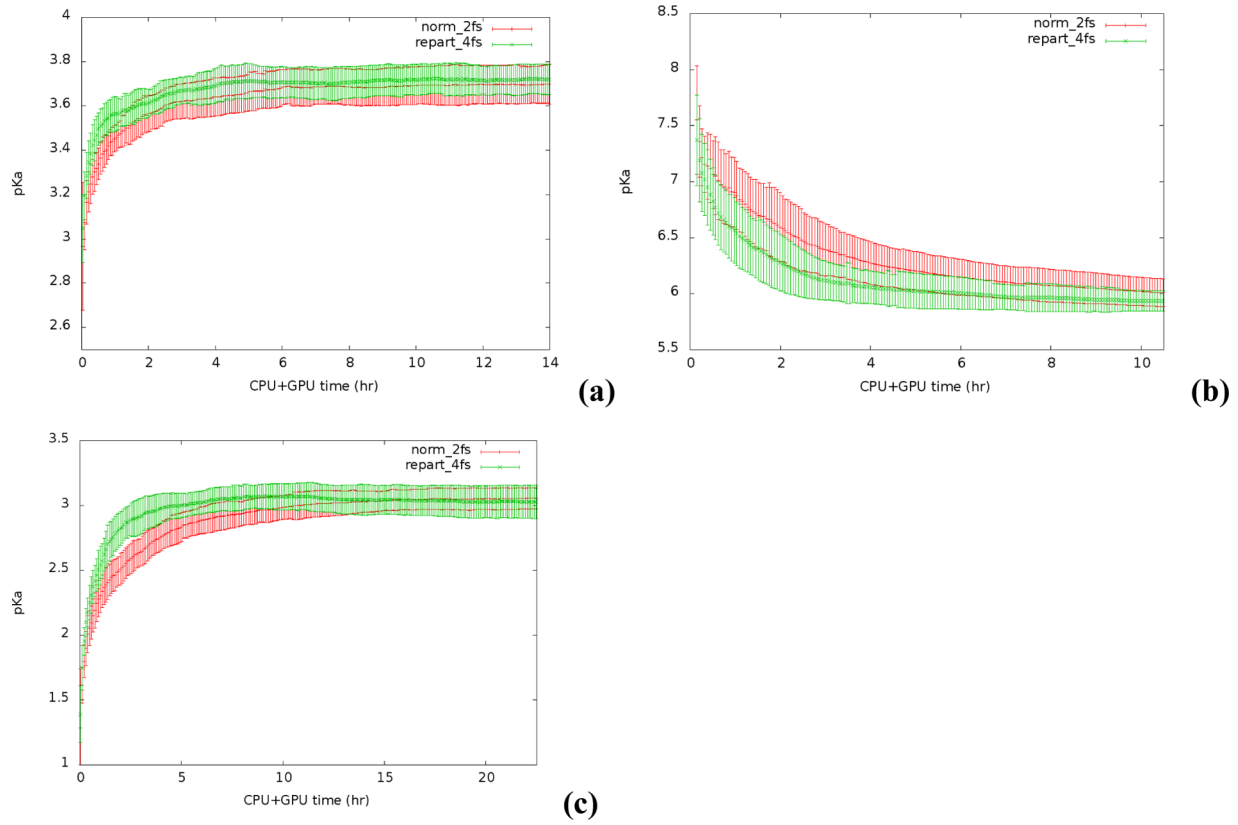

Figure 14. Evolution of calculated pK_a values using constant pH MD on HEWL for two different trajectory types in 3 of the 10 residues treated: (a) GLU7, (b) HIS15, and (c) ASP87. Error bars are from averaging over 20 independent trajectories in each pH for each trajectory type.

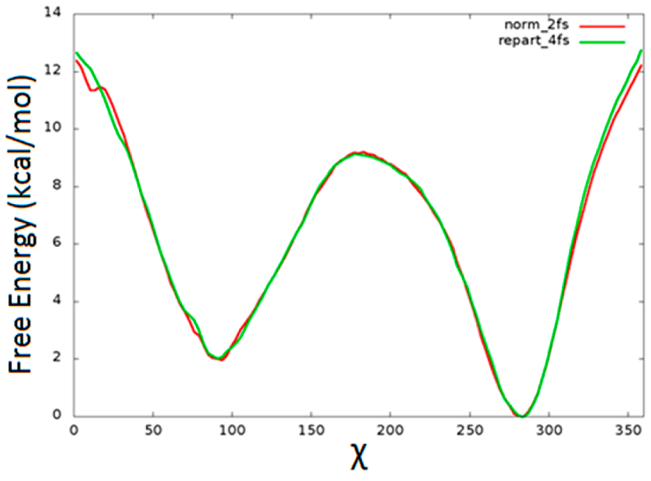

Figure 15. PMF for rotation about the dihedral χ in the MTS spin label, generated through umbrella sampling.

settings, we observed that SHAKE failure typically occurred before any significant problems from energy conservation breaking down arose. Here, we would like to focus on the mechanics by which HMR preserves simulation stability beyond SHAKE's capabilities. SHAKE is used to effectively freeze the fast bond vibrations involving hydrogen atoms in the solute, so it would initially seem odd that HMR applied to the solute hydrogens provides any further stabilization over the application of SHAKE by itself. As previously mentioned, the 2-fs time step limit that comes with the use of SHAKE is derived from limitations within the SHAKE algorithm itself and is not a fundamental limit, because of high-frequency motions such as the original 1-fs limit. Beyond 2 fs, for large systems, there is a high chance of SHAKE failing due to the algorithm's limitations (this is somewhat dependent on the exact tolerance settings used, so the discussion that follows assumes default Amber SHAKE settings). The source of this limitation can be understood by briefly exploring how the SHAKE algorithm works. In what follows, we will consider the case of a single round of SHAKE involving only two atoms (e.g., a C_α/H_α pair), referring to Figure 16.

During an iteration of SHAKE, as implemented in Amber, the two atoms (A and B) are moved back to the target distance (R_0) along the axis connecting them in the previous MD step (z). We consider two cases from the perspective of atom A (i.e.,

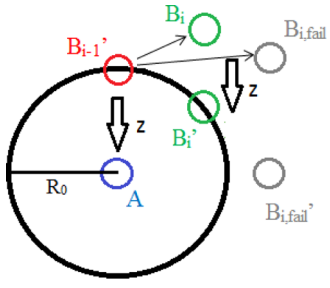

Figure 16. Graphic representation of a round of the SHAKE algorithm. The distance between the two atoms (labeled A and B) at the end of the previous MD step is R_0. Two cases are shown: in one case, atom B moves a small distance in the current MD step to B_i, and is moved along the original z-axis back to a distance of R_0 at B_i'. In the other case, atom B moves a farther distance to $B_{i,fail}$, at which point it is not possible to move back to a distance R_0 along the z-axis.

DOI: 10.1021/ct5010406
J. Chem. Theory Comput. 2015, 11, 1864−1874

atom A does not move): for the first case, the SHAKE algorithm is able to successfully move atom B back to the original distance. This case is shown in green in Figure 16. However, it is possible that atom B moves far enough in a given direction away from atom A that it is not possible to move the atom back to a distance R_0 along the z-axis (shown in gray). What happens at this point is implementation-dependent. For example, in the CPU version of Amber 14, the simulation will exit in this case with an error. However, in the GPU version, for efficiency reasons, the simulation will continue even though the SHAKE iteration did not successfully converge. With the usual tolerance settings on large systems, this quickly leads to instabilities that manifest as the simulation "blowing up." Obviously, with an increase in time step, the distance moved by each atom between each run of SHAKE is increased on average, leading to a larger probability of the "gray" case. The application of HMR damps this increase in average instantaneous displacement from MD step to MD step in the hydrogen atoms, leading to a decrease in the probability of this SHAKE failure.

For each topology, there was a "border" time step, where the simulation experienced SHAKE instabilities after more than a few MD steps, but still on the order of tens of nanoseconds. For instance, for HEWL, the border was 4 fs for norm and 5 fs for repart and repart_water. In this system, the norm/4 fs trajectories ran, at most, until 14 ns before experiencing SHAKE instabilities, with most failing before 10 ns, while the repart/5 fs and repart_water/5 fs trajectories ran for, at most, 1 ns before failing. The role of HMR in extending the stability of systems (with respect to SHAKE) to longer time steps is in pushing this "border" of SHAKE instability to longer time steps without affecting conformational space.

V. CONCLUSION

Two main problems face the researcher when using molecular dynamics (MD) as a tool to study atomic-level dynamics of large biomolecular systems; these are typically called the "force field problem" and the "sampling problem." The force field problem refers to inaccuracies in the coarse molecular mechanics level of theory used in classical force fields; this problem is continually combated with the derivation of high-quality force field parameters using high level ab initio and experimental data, in order to bring the force field potential energy surface being sampled into better agreement with physical reality. The sampling problem refers to the infeasibility of running simulations long enough to sufficiently sample long-time scale (i.e., much longer than microseconds) events that form the basis of many important biological processes. This problem is constantly being chipped away at with incremental improvements in hardware, and this, combined with algorithmic improvements and increased use of parallelism (e.g., GPUs), continues to unlock routine access to longer time scales for study with MD. In this work, we have examined a technique that allows MD simulations, as well as advanced sampling techniques based on MD-like umbrella sampling and constant pH MD, to be accelerated by a factor of ∼2. We have also explored, in some small detail, how HMR stabilizes the system on top of the SHAKE algorithm. As shown, the application of HMR with long-time-step MD trajectories does not introduce significant additional error, compared to the "usual" case of 2-fs trajectories with normal masses. In addition, HMR does not place any significant overhead on the user; it is trivial to incorporate mass-repartioned topologies into existing simulation setups.

One interesting remaining point for further study is more fully exploring the relative utility of the "repart" topology type versus the "repart_water" type; i.e., what advantages and disadvantages there are to applying HMR to the solvent atoms with the increased time step. Our results here indicate that the time step can be doubled in a stable fashion without repartitioning the masses of the TIP3P model, which avoids increasing the viscosity of the system and thus decreasing the sampling efficiency of the trajectory. This is due to the application of the analytic SETTLE algorithm in this water model; this algorithm does not suffer the same limitations as the iterative SHAKE. However, leaving the water molecules unchanged while increasing the time step leads to (i) more sampling of unfavorable configurations, because of the less-accurate integration of the librational movement in the water molecules, and (ii) higher stress in the solvent distribution. If the protein sampling is truly unaffected, as our results seem to indicate, then this would be the preferred simulation setup for protein studies as solute sampling efficiency is then truly doubled without the viscosity damping effect. A possible alternative to this approach could be to apply an overall mass scaling to only the solvent molecules after applying HMR, decreasing the total solvent mass, and thus lowering the system viscosity. Lin and Tuckerman[45] recently investigated a similar method as applied to peptide simulations. Although, as previously mentioned, the time scale of the solvent motion would be affected, it is possible that this type of setup would allow an accelerated sampling of the protein motion without the viscosity effect.

AUTHOR INFORMATION

Corresponding Author

*E-mails: roitberg@ufl.edu, roitberg@qtp.ufl.edu.

Notes

The authors declare no competing financial interest.

ACKNOWLEDGMENTS

We would like to thank Carlos Simmerling and Tom Cheatham for their own tests on long-time-step HMR MD. This research is part of the Blue Waters Sustained-Petascale Computing Project, which is supported by the National Science Foundation (Award No. OCI 07-25070) and the state of Illinois. Blue Waters is a joint effort of the University of Illinois at Urbana−Champaign and its National Center for Supercomputing Applications. Research funding comes from National Science Foundation (No. OCI-1147910). The authors thank the High-Performance Computing Center at the University of Florida for providing further computational resources.

REFERENCES

(1) Pierce, L. C. T.; Salomon-Ferrer, R.; Augusto F. de Oliveira, C.; McCammon, J. A.; Walker, R. C. *J. Chem. Theory Comput.* **2012**, *8*, 2997−3002.
(2) Schaeffer, R. D.; Fersht, A.; Daggett, V. *Curr. Opin. Struct. Biol.* **2008**, *18*, 4−9.
(3) Stone, J. E.; Hardy, D. J.; Ufimtsev, I. S.; Schulten, K. *J. Mol. Graph. Model.* **2010**, *29*, 116−125.
(4) Götz, A. W.; Williamson, M. J.; Xu, D.; Poole, D.; Le Grand, S.; Walker, R. C. *J. Chem. Theory Comput.* **2012**, *8*, 1542−1555.
(5) Kubelka, J.; Hofrichter, J.; Eaton, W. A. *Curr. Opin. Struct. Biol.* **2004**, *14*, 76−88.

DOI: 10.1021/ct5010406
J. Chem. Theory Comput. 2015, 11, 1864−1874

(6) Christ, C. D.; Mark, A. E.; van Gunsteren, W. F. *J. Comput. Chem.* **2010**, *31*, 1569−1582.
(7) Hansen, H. S.; Hünenberger, P. H. *J. Comput. Chem.* **2010**, *31*, 1−23.
(8) Case, D. A.; Babin, V.; Berryman, J.; Betz, R. M.; Cai, Q.; Cerutti, D. S.; Cheatham III, T. E.; Darden, T. A.; Duke, R. E.; Gohlke, H.; Goetz, A. W.; Gusarov, S.; Homeyer, N.; Janowski, P.; Kaus, J.; Kolossváry, I.; Kovalenko, A.; Lee, T. S.; LeGrand, S.; Luchko, T.; Luo, R.; Madej, B.; Merz, K. M.; Paesani, F.; Roe, D. R.; Roitberg, A.; Sagui, C.; Salomon-Ferrer, R.; Seabra, G.; Simmerling, C. L.; Smith, W.; Swails, J.; Walker, R. C.; Wang, J.; Wolf, R. M.; Wu, X.; Kollman, P. A. *AMBER 14*, 2014.
(9) Ryckaert, J.-P.; Ciccotti, G.; Berendsen, H. J. *J. Comput. Phys.* **1977**, *23*, 327−341.
(10) Miyamoto, S.; Kollman, P. A. *J. Comput. Chem.* **1992**, *13*, 952−962.
(11) Mazur, A. K. *J. Comput. Phys.* **1997**, *136*, 354−365.
(12) Engle, R. D.; Skeel, R. D.; Drees, M. *J. Comput. Phys.* **2005**, *206*, 432−452.
(13) Skeel, R. D.; Hardy, D. J. *SIAM J. Sci. Comput.* **2001**, *23*, 1172−1188.
(14) Gans, J.; Shalloway, D. *Phys. Rev. E* **2000**, *61*, 4587−4592.
(15) Hünenberger, P. H. *Adv. Polym. Sci.* **2005**, *173*, 105−149.
(16) Bussi, G.; Parrinello, M. *Phys. Rev. E* **2007**, *75*, 056707.
(17) Melchionna, S. *J. Chem. Phys.* **2007**, *127*, 044108.
(18) Jacucci, G.; Rahman, A. *Report on Workshop Methods in Molecular Dynamics—Long Timescale Events*, Orsay, France, 1974; pp 32−40.
(19) Bennett, C. H. *J. Comput. Phys.* **1975**, *19*, 267−279.
(20) *Water: A Comprehensive Treatise*; Franks, F., Ed.; Springer: Boston, MA, 1979; p 279.
(21) Pomès, R.; McCammon, J. A. *Chem. Phys. Lett.* **1990**, *166*, 425−428.
(22) Mao, B.; Friedman, A. R. *Biophys. J.* **1990**, *58*, 803−805.
(23) Mao, B.; Maggiora, G. M.; Chou, K. C. *Biopolymers* **1991**, *31*, 1077−1086.
(24) Mao, B. *Biophys. J.* **1991**, *60*, 611−622.
(25) Feenstra, K. A.; Hess, B.; Berendsen, H. J. C. *J. Comput. Chem.* **1999**, *20*, 786−798.
(26) Hess, B.; Kutzner, C.; van der Spoel, D.; Lindahl, E. *J. Chem. Theory Comput.* **2008**, *4*, 435−447.
(27) Harvey, M. J.; Giupponi, G.; Fabritiis, G. De. *J. Chem. Theory Comput.* **2009**, *5*, 1632−1639.
(28) Rao, F.; Spichty, M. *J. Comput. Chem.* **2012**, *33*, 475−483.
(29) Salomon-Ferrer, R.; Götz, A. W.; Poole, D.; Le Grand, S.; Walker, R. C. *J. Chem. Theory Comput.* **2013**, *9*, 3878−3888.
(30) Le Grand, S.; Götz, A. W.; Walker, R. C. *Comput. Phys. Commun.* **2013**, *184*, 374−380.
(31) Cornell, W. D.; Cieplak, P.; Bayly, C. I.; Gould, I. R.; Merz, K. M.; Ferguson, D. M.; Spellmeyer, D. C.; Fox, T.; Caldwell, J. W.; Kollman, P. A. *J. Am. Chem. Soc.* **1995**, *117*, 5179−5197.
(32) Hornak, V.; Abel, R.; Okur, A.; Strockbine, B.; Roitberg, A.; Simmerling, C. *Proteins* **2006**, *65*, 712−725.
(33) Wang, J.; Wolf, R. M.; Caldwell, J. W.; Kollman, P. A.; Case, D. A. *J. Comput. Chem.* **2004**, *25*, 1157−1174.
(34) Bayly, C. I.; Cieplak, P.; Cornell, W.; Kollman, P. A. *J. Phys. Chem.* **1993**, *97*, 10269−10280.
(35) Frisch, M. J.; Trucks, G.; Schlegel, H. B.; Scuseria, G. E.; Robb, M. A.; Cheeseman, J. R.; Scalmani, G.; Barone, V.; Mennucci, B.; Petersson, G. A.; Nakatsuji, H.; Caricato, M.; Li, X.; Hratchian, H. P.; Izmaylov, A. F.; Bloino, J.; Zheng, G.; Sonnenberg, J. L.; Hada, M.; Ehara, M.; Toyota, K.; Fukuda, R.; Hasegawa, J.; Ishida, M.; Nakajima, T.; Honda, Y.; Kitao, O.; Nakai, H.; Vreven, T.; Montgomery, J. A. J.; Peralta, J. E.; Ogliaro, F.; Bearpark, M.; Heyd, J. J.; Brothers, E.; Kudin, K. N.; Staroverov, V. N.; Kobayashi, R.; Normand, J.; Raghavachari, K.; Rendell, A.; Burant, J. C.; Iyengar, S. S.; Tomasi, J.; Cossi, M.; Rega, N.; Millam, J. M.; Klene, M.; Knox, J. E.; Cross, J. B.; Bakken, V.; Adamo, C.; Jaramillo, J.; Gomperts, R.; Stratmann, R. E.; Yazyev, O.; Austin, A. J.; Cammi, R.; Pomelli, C.; Ochterski, J. W.; Martin, R. L.; Morokuma, K.; Zakrzewski, V. G.; Voth, G. A.; Salvador, P.; Dannenberg, J. J.; Dapprich, S.; Daniels, A. D.; Farkas, O.; Foresman, J. B.; Ortiz, J. V.; Cioslowski, J.; Fox, D. J. *Gaussian 09*; Gaussian, Inc.: Wallingford, CT, 2009.
(36) Hopkins, C. W.; Roitberg, A. E. *J. Chem. Inf. Model.* **2014**, *54*, 1978−1986.
(37) Roe, D. R.; Cheatham, T. E. *J. Chem. Theory Comput.* **2013**, *9*, 3084−3095.
(38) Jorgensen, W. L.; Chandrasekhar, J.; Madura, J. D.; Impey, R. W.; Klein, M. L. *J. Chem. Phys.* **1983**, *79*, 926.
(39) Young, A. C. M.; Dewan, J. C.; Nave, C.; Tilton, R. F. *J. Appl. Crystallogr.* **1993**, *26*, 309−319.
(40) Mongan, J.; Case, D. A.; McCammon, J. A. *J. Comput. Chem.* **2004**, *25*, 2038−2048.
(41) Ding, F.; Layten, M.; Simmerling, C. *J. Am. Chem. Soc.* **2008**, *130*, 7184−7185.
(42) Sezer, D.; Freed, J. H.; Roux, B. *J. Phys. Chem. B* **2008**, *112*, 5755−5767.
(43) Pedretti, A.; Villa, L.; Vistoli, G. *J. Comput. Aided. Mol. Des.* **2004**, *18*, 167−173.
(44) Roux, B. *Comput. Phys. Commun.* **1995**, *91*, 275−282.
(45) Lin, I.-C.; Tuckerman, M. E. *J. Phys. Chem. B* **2010**, *114*, 15935−15940.

DOI: 10.1021/ct5010406
J. Chem. Theory Comput. 2015, 11, 1864−1874